2011-08

Experimental and theoretical investigation of molecular structure and conformation of the 4-isopropylthioxanthone

Journal of Molecular Structure, Amsterdam : Elsevier BV, v. 1000, n. 1/3, p. 155-161, Aug. 2011
http://www.producao.usp.br/handle/BDPI/49615

Journal of Molecular Structure 1000 (2011) 155–161

Contents lists available at ScienceDirect

Journal of Molecular Structure

journal homepage: www.elsevier.com/locate/molstruc

Experimental and theoretical investigation of molecular structure and conformation of the 4-isopropylthioxanthone

Rodrigo S. Corrêa [a,b,*], João P. Barolli [b], Leandro Ribeiro [a], Alzir A. Batista [b], Javier Ellena [a], Marcelo B. Andrade [a,*]

[a] Departamento de Física e Informática, Instituto de Física de São Carlos, Universidade de São Paulo, Caixa Postal 369, CEP 13560-970, São Carlos, SP, Brazil
[b] Departamento de Química, Universidade Federal de São Carlos – UFSCar, Rodovia Washington Luiz, KM 235 CP 676, CEP 13561-901, São Carlos, SP, Brazil

ARTICLE INFO

Article history:
Received 23 February 2011
Received in revised form 7 June 2011
Accepted 13 June 2011
Available online 6 July 2011

Keywords:
Isopropylthioxanthones
Photoinitiator
Molecular conformation
Intermolecular interactions
Theoretical calculations
Spectroscopy analyses

ABSTRACT

In this study, the molecular structure and conformational analyses of the 4-isopropylthioxanthone (4-ITX) are reported according to experimental and theoretical results. The compound crystallizes in the centrosymmetric $P\bar{1}$ space group with only one molecule in the asymmetric unit, presenting the most stable conformation, in which the three fused-rings adopt a planar geometry, and the isopropyl group assumes a torsional angle with less sterical hindrance. The structural and conformational analyses were performed using theoretical calculations such as Hartree–Fock (HF), DFT method in combination with 6-311G(d,p) and 6-31++G(d,p) and the results were compared with infrared spectroscopy (FT-IR) and X-ray diffraction (XRD). The supramolecular assembly of 4-ITX is kept by non-classical C–H···O hydrogen bonds and weak interactions such as π–π stacking. 4-ITX was also studied by ^{1}H and ^{13}C NMR spectroscopy. UV–Vis absorption spectroscopic properties of the 4-ITX showed the long-wavelength maximum shifts towards high energy when the solvent polarity increases.

1. Introduction

Thioxanthone (TX) derivatives are widely studied due to their photochemistry and their vital role in photopolymerization activity [1–3]. Previous studies have presented the free radical polymerization of olefinic compounds photoinitiated by TX and their derivatives, which are sensitive to the quenching of the excited triplet states that react with a hydrogen donor thereby producing an initiating radical. The mentioned quenching effect is the reactive precursor of light-induced chemical changes in carbonyl groups [4]. This process occurs mainly because TX derivatives absorb at a longer UV wavelength region than other well known photoinitiators ensuring efficient light absorption during the UV-curing process for a number of materials such as adhesives and printing inks [5].

A specific class known as isopropylthioxanthone (ITX) has been used in the printing process of the packaged food cartons. Since 2005, when a mixture of 2- and 4-isopropylthioxanthone was detected in baby milk, authorities have been aware of the risks of ITX for human health and have fostered studies on the analytical field to develop new methods for the determination of both 2- and 4-ITX isomers in foods, for which the technique of liquid chromatography/tandem mass spectrometry has been used [6,7]. In addition, antitumor and cytotoxic are interesting pharmacological activities exhibited by TX derivatives. Previous studies have investigated the *in vivo* efficacy of SR 233377 derivatives against the murine solid tumor Panc03 [8]. Recently, a promising thioxanthone analog of third-generation, SR 271425, has presented antitumor activity against a wide range of tumor types, and it already is in phase I studies [9].

Even though many studies about the photochemical and pharmacological activities of thioxanthone derivatives are found in literature, there are few reports dealing with their structural and chemical properties, including X-ray diffraction (XRD) analysis, spectroscopic techniques, and theoretical calculations. Therefore, the aim of this study is to report a detailed structural investigation of 4-isopropylthioxanthone (4-ITX). The structure was solved by single-crystal XRD, and its molecular conformation and the crystal self-assembly were analyzed. The geometrical parameters obtained were compared with similar structures deposited in the Cambridge Structural Database (CSD). In addition, theoretical calculations were performed using *ab initio* molecular orbital procedures [Hartree–Fock (HF)], density functional theory (B3LYP) in combination with the 6-311G(d,p), and 6-31++G(d,p) basis sets in order to compare with XRD and infrared (IR) spectroscopy results.

* Corresponding authors. Address: Departamento de Química, Universidade Federal de São Carlos – UFSCar, Rodovia Washington Luiz, KM 235 CP 676, CEP 13561-901, São Carlos, SP, Brazil (R.S. Corrêa). Tel.: +55 16 3373 8096; fax: +55 16 3373 9777.
E-mail addresses: rodrigocorrea@ufscar.br (R.S. Corrêa), mabadean@terra.com.br (M.B. Andrade).

0022-2860/$ - see front matter © 2011 Elsevier B.V. All rights reserved.
doi:10.1016/j.molstruc.2011.06.016

The ^1H and $^{13}C\{^1H\}$ NMR technique and UV–Vis absorption were performed to investigate the behavior of the 4-ITX in solution.

2. Experimental

2.1. Measurements and computational details

The sample of 4-ITX was purchased from Sigma/Aldrich and used without further purification. The IR spectrum of the compound was recorded on a FT-IR Bomem-Michelson 102 spectrometer in the 4000–400 cm^{-1} region using solid samples pressed in KBr pellets. UV–Vis spectra were recorded in a HP8452A (diode array) spectrophotometer. Dilutions of 1.0×10^{-4} mol L^{-1} in dichloromethane, tetrahydrofuran, and methanol were prepared, and quartz cells of 1.0 cm path length were used in the analysis. The ^1H and $^{13}C\{^1H\}$ spectra were recorded in $CDCl_3$ solution in a 5 mm sample tube at 293 K on a Bruker Avance III DRX 400 spectrometer working at 400 and 100 MHz, respectively. The splitting patterns of proton resonance are designated as d = duplet, dd = double doublet, dt = double triplet, sep = septet, m = multiplet (the NMR assignments follow the crystallographic numbering system). ^1H NMR (δ): 8.60 (dt, 1H, J = 0.96 and 0.80 Hz; H_1), 8.55 (dd, 1H, J = 1.52, 1.48 Hz; H_8), 7.64–7.61 (m, 3H; H_2 and H_7); 7.51–7.47 (m, 2H; H_3 and H_6); 3.49 (sep, 1H, J = 6.76 Hz; H_{41}); 1.40 (d, 6H, J = 6.76 Hz; H_{42} and H_{43}). $^{13}C\{^1H\}$ NMR (δ): 180.77, 144.62, 136.96, 135.41, 132.24, 129.80, 129.62, 128.91, 128.62, 127.87, 126.33, 30.03, and 23.00.

All calculations were performed with Gaussian 03 W [10] program package using an AMD Phenon II X4 965 Quad Core processor with 4 GB Ram. We used the Hartree–Fock (HF) [11] and density functional theory (DFT) [12] with the three parameters hybrid functional of BECK (B3), for the exchange part, and the Lee, Yang, and Parr (LYP) correlation function [13,14] using 6-31++G and 6-311G(d,p) basis sets in order to obtain the vibrational frequencies of the IR spectra, scanning of potential energy as a function of dihedral angle, optimized energies, and thermodynamic parameters.

2.2. X-ray crystallographic analysis

Single crystals of 4-ITX were grown by recrystallization in a methanol solution at room temperature. To perform the X-ray diffraction experiment, a suitable single crystal was mounted on glass fiber, and positioned on the goniometer head. Intensity data were measured with the crystal at 150 K using the Enraf–Nonius Kappa-CCD diffractometer with graphite monochromated Mo Kα radiation (λ = 0.71073 Å). The cell refinements were performed using the software Collect [15] and Scalepack [16], and the final cell parameters were obtained on all reflections. Data reduction was carried out using the software Denzo-SMN and Scalepack [16].

The structure was solved by the Direct method using SHELXS-97 [17] and refined using the software SHELXL-97 [17]. Non-hydrogen atoms of 4-ITX were unambiguously located, and a full-matrix, least-squares refinement of these atoms with anisotropic thermal parameters was carried out. The C–H hydrogen atoms were positioned stereochemically and were refined with fixed individual displacement parameters [$U_{iso}(H) = 1.2U_{eq}$ (C^2_{sp}) or $1.5U_{eq}$ (C^3_{sp})] using a riding model with aromatic, methyl, and methyne C–H bond lengths were fixed of 0.93, 0.96, and 0.98 Å, respectively. Tables were generated by WinGX [18] and the structure representations by ORTEP-3 [19] and MERCURY [20]. The intramolecular parameters (bond lengths, valence angles, and acyclic torsion angles) were analyzed using MOGUL [21], a knowledge base of molecular geometry derived from Cambridge Structural Database (CSD, Version 1.12, update August 2010, [22]). Hirshfeld surface for 4-ITX was calculated using the CrystalExplorer 2.1 program [23] to illustrate the main differences between the intermolecular contacts in the crystal structure. Table 1 summarizes the main crystal data collections and structure refinement parameters for the thioxanthone derivative under study.

Table 1
Crystal data and structure refinement for 4-ITX.

Compound	4-ITX
Empirical formula	$C_{16}H_{14}OS$
Formula weight	254.33
Temperature (K)	150
Crystal system	Triclinic
Space group	$P\bar{1}$
Unit cell dimensions (Å, °)	a = 7.3957(3); α = 90.215(2) b = 8.0442(3); β = 103.037(2) c = 10.6912(4); γ = 96.033(2)
Volume (Å^3)	615.97(4)
Z	2
Density (calculated) (Mg m^{-3})	1.371
Absorption coefficient (mm^{-1})	0.246
F(0 0 0)	268
Crystal size (mm^3)	0.12 × 0.14 × 0.18
θ range for data collection (°)	3.06–26.35
Index ranges	$-8 \leqslant h \leqslant 9$, $-10 \leqslant k \leqslant 10$, $-13 \leqslant l \leqslant 13$
Reflections collected	4364
Independent reflections	2497 [R(int) = 0.0407]
Completeness to θ_{max}	99.7%
Refinement method	Full-matrix least-squares on F^2
Data/restraints/parameters	2497/0/165
Goodness-of-fit on F^2	1.082
Final R indices [I > 2sigma(I)]	R1 = 0.0475, wR2 = 0.1042
R indices (all data)	R1 = 0.0634, wR2 = 0.1094
Largest diff. peak and hole (e Å^{-3})	0.321 and −0.362

3. Results and discussion

3.1. Structural analysis

The structural study performed by XRD pointed out that 4-ITX crystallizes in a centrosymmetric $P\bar{1}$ space group with only one molecule in the asymmetric unit (Fig. 1). With regard to the intramolecular conformation of 4-ITX, it is observed that the three fused-rings adopt an almost planar conformation, which agrees with other thioxanthone structures reported previously [24]. Comparing with similar structures, planarity also can be observed to the thioxanthone S,S-dioxide derivative named thioxanthone-10,10-dioxide [25], whereas small folding angles are present in the 2,4-dimethylthioxanthone-10,10-dioxide [26]. On the other hand, molecules containing thioxanthone S-oxide core present the central ring strongly distorted with the sulfur atom on center of a trigonal pyramidal geometry [27].

To emphasize the planar tendency of the thioxanthone core, a careful analysis was performed by the root mean of square deviation (RMSD) from the least-squares plane through the rings A, B, and C of the 4-ITX. All atoms in the rings A, B, and C lie within 0.0505 Å of the least squares plane through the three-ring system. Each ring is also almost planar, including the C41 atom linked to ring A. The largest deviations from the individual least-squares planes are 0.0058, 0.0074, and 0.0254 Å for rings A, B, and C, respectively. The least squares planes of the rings A and C form a dihedral angle of 2.55(6)°, those of the rings B and C form an angle of 1.98(6)°, and those of the A and B rings form an angle of 4.40(7)°. As observed and studied previously, the chromene central ring is the most susceptible to distortion [28].

An analysis of the molecular structure of 4-ITX shows that the isopropyl group linked at C4 atom is presenting the conformation close to lower energy, when compared with the structure optimized by theoretical calculation performed in this paper. In the

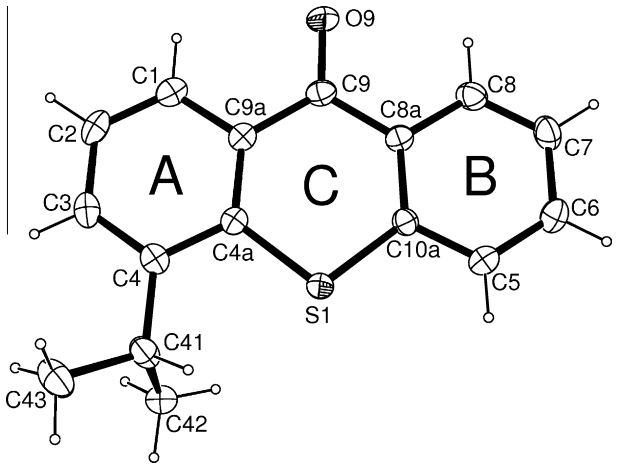

Fig. 1. ORTEP-3 plot of 4-ITX showing the non-hydrogenous atoms and the rings labeled. The ellipsoids are represented at 50% probability level, and the H-atoms are shown as spheres of arbitrary radii.

molecule this group presents freedom to rotate around C4–C41 bond. The conformational analyses were performed after the calculations of the gradient optimization and vibrational modes of IR. The potential energy curve of 4-ITX was calculated ranging the C4a–C4–C41–C43 torsion angle, ϕ, from $-180°$ to 180° with a step of 10°. The results present a total of three minimum and two maximum (Table S1 and Fig. S2, in Supplementary material). The two regions presenting states of maximum energies ($-140°$ and 20°) can be explained by electrostatic repulsion between the methyl groups (C42 and C43) and the S1 atom. The global minimum was observed at 90°, presenting absolute energy of -2868315.971 kJ mol^{-1}, whereas the other two minima at $\phi = 140°$ and $\phi = -70°$ present energy values slightly higher, with relative energy of 0.066 kJ mol^{-1} and 11.058 kJ mol^{-1}, respectively. The energies values found in $\phi = 90°$ and $\phi = 140°$ are almost similar. As observed, the three minima values obtained by the scan do not agree with C4a–C4–C41–C43 torsion angle found in the crystal structure [153.8(2)°]. Such deviation probably occurs due to the influence of intermolecular hydrogen bonds discussed below in this paper.

The main bond lengths and angles obtained by X-ray diffraction and theoretical experiments are given in Table 2. These parameters were compared using the program Mogul [20], which allows us to compare the experimental bond lengths, bond angles, and torsion angles of a given compound with those found in similar structures which are deposited in the CSD [22]. Mogul statistic revealed that all bond lengths and bond angles values for 4-ITX agree with those found for similar compounds studied by X-ray diffraction (Table S2 and S3, in Supplementary material). The values of C–C bond distances within the A and B benzyl rings range 1.369(3)–1.414(3) Å, which agree well with the normal aromatic value [1.39(1) Å]. Meanwhile the C–C bond distances for the optimized structure are ranging 1.388–1.419 Å, 1.403–1.418 Å and 1.397–1.409 Å, respectively, for the HF/6-311G(d,p), B3LYP/6-31++G and B3LYP/6-311G(d,p) methods. Similarly, the mean bond angles in rings A and B are 120(2)°. The isopropyl parameters follow the same behavior expected. In the literature, the average value of the C–S bond length is 1.76(1) Å, which agree with that one found in ring C for C4a–S1 [1.747(2) Å] and C10a–S1 [1.734(2) Å] bond length. The C9=O9 fragment presents a small shift compared to the other double bonds of similar crystal structures deposited in the CSD, which present the mean value of 1.226(21) Å (Table 2). This can be an effect of intermolecular hydrogen bonding and delocalization of the π-system involving the carbonyl and the ring C. For example, an electron delocalization involving the moiety S1–C4a–C9a–C9–O9 atoms and also the fragment S1–C10a–C8a–C9–O9. To emphasize the resonance effect, the S1–C4a, S1–C10a, C9a–C9, and C8a–C9 single bonds are slight shorter than the average values found for these geometric parameters (Table 2), contributing to keep the molecule in a flat conformation. In most cases, the theoretical studies reported that the HF method generally underestimates the values of bond lengths, while the DFT method provides the geometric parameters closer to experimental data. For this reason, we must take into account the DFT method for the structural data. Although there are some differences between the experimental and theoretical values, it is shown that the experimental results can be reproduced by procedure of optimizing methods. Thus, using three methods, Tables 2 shows a comparison of the calculated geometrical parameters for 4-ITX with the experimental structure obtained from X-ray diffraction by means of the root-mean square deviation (RMSD) values. According to these results, the basis set that best reproduces the theoretical geometrical parameters for the compound is B3LYP/6-311G(d,p), in which the mean differences for the bond length are 0.011, 0.012 and 0.030 Å for the B3LYP/6-311G(d,p), HF/6-311G(d,p) and B3LYP/6-31++G methods, respectively, while for the bond angles the values are 0.5, 0.6 and 0.7° (Table 2).

The supramolecular investigation of 4-ITX shows that classical intermolecular hydrogen bonds were not present due to the absence of a strong proton donor. Thus, there are only non-classical hydrogen bonds. An important hydrogen bond that contribute for the crystal packing stabilization involves the C5–H5···O9 atoms, which form a one-dimensional infinite ribbon along the [010] direction (Fig. 2, Table 3). In addition, the 1-D chains are linked by van der Waals interactions involving mainly the isopropyl group, such as the one illustrated in Fig. 2 with a gray line in zigzag.

A surprising result related to the intermolecular analysis of 4-ITX is that the crystal self-assembly of this compound is similar to another thioxanthone derivative known as 4-methylthioxanthone (4-MTX) [24]. The main intramolecular difference between both thioxanthone derivatives is the substituent linked at C4 atom, which it is an isopropyl group in the 4-ITX, whereas it is a methyl group in the 4-MTX molecule. As observed by the crystallographic analysis, both structures are isomorphic, that means, they crystallize in the same $P\bar{1}$ space group with similar cell parameters and crystal assembly. For 4-MTX, the unit cell parameters [$a = 7.118(1)$ Å, $b = 7.907(2)$ Å and $c = 10.415(2)$ Å; $\alpha = 77.74(1)°$, $\beta = 74.35(1)°$, and $\gamma = 73.96(1)°$] are smaller than the values of 4-ITX. The compression of the unit cell parameters is expected because the different volume of substituents linked to the position 4. In a recent paper, we reported a similar behavior of isomorphism occurring in natural products, such as the case of Lupeol [29], a pentacyclic triterpene derivative. Lupeol proved isomorphic to 3β,30-dihydroxylup-20(29)-ene [30], which differs chemically due to an additional hydroxyl group.

Another weak intermolecular interaction is represented by C42–H42···O9 [the C···O distance is 3.387 Å] forming a dimer (Fig. 3a). As observed, this interaction plays an important role in stabilizing the conformation of the isopropyl group thus justifying the slight deviation related to the theoretical calculation results. Also, a common kind of interaction occurring in resonant three-fused rings [28] can be seen in Fig. 3b. The molecules are face-to-face π-stacked forming dimer, in which the planes of thioxanthone rings are strictly parallel to each other. They also present a displacement angle between their centers of about 19.5°. The center to center distance between Cg1 and Cg3 is 3.631(1) Å with an interplanar separation of 3.460(1) Å.

Therefore, for the whole crystal packing stabilization of 4-ITX, weak intermolecular contacts (H···H, C···C and H···H) together with the hydrogen bonds are necessary. The analysis of the Hirsh-

Table 2
Experimental and theoretical bond lengths and bond angles obtained for 4-ITX.

Bond length (Å)	X-ray	Mogul Values	B3LYP 6-31++G	B3LYP 6-311G(d,p)	HF 6-311G(d,p)
O9–C9	1.231 (3)	1.226	1.260	1.226	1.195
S1–C10a	1.734 (2)	1.759	1.817	1.759	1.756
S1–C4a	1.747 (2)	1.762	1.832	1.772	1.768
C1–C2	1.369 (3)	1.386	1.387	1.380	1.370
C2–C3	1.391 (3)	1.386	1.403	1.397	1.388
C3–C4	1.385 (3)	1.392	1.401	1.392	1.382
C4–C41	1.521 (3)	1.518	1.531	1.526	1.528
C41–C42	1.532 (3)	1.520	1.550	1.542	1.536
C41–C43	1.528 (3)	1.520	1.544	1.538	1.534
C5–C6	1.374 (3)	1.386	1.393	1.384	1.372
C6–C7	1.396 (3)	1.374	1.407	1.402	1.394
C7–C8	1.370 (3)	1.386	1.390	1.382	1.371
C8–C8a	1.404 (3)	1.394	1.415	1.408	1.400
C8a–C9	1.478 (3)	1.478	1.481	1.484	1.486
C10a–C8a	1.396 (3)	1.403	1.405	1.403	1.385
C10a–C5	1.400 (3)	1.396	1.407	1.406	1.398
C4a–C9a	1.406 (3)	1.408	1.412	1.409	1.394
C9a–C9	1.475 (3)	1.478	1.486	1.490	1.493
C9a–C1	1.403 (3)	1.394	1.413	1.405	1.396
C4a–C4	1.414 (3)	1.405	1.419	1.418	1.409
RMSD			0.030	0.011	0.012
Bond angles (°)					
C10a–S1–C4a	104.5 (1)	101.412	103.1	104.3	104.6
C10a–C8–C9	123.7 (2)	123.747	124.1	123.8	123.5
C10a–C8a–C8	118.4 (2)	118.792	118.3	118.5	119.0
C9–C8a–C8	117.9 (2)	119.274	117.6	117.7	118.0
S1–C10a–C8a	124.4 (2)	121.899	123.9	124.4	124.5
S1–C10a–C5	115.7 (2)	118.337	115.5	115.5	115.5
C8a–C10a–C5	119.9 (2)	119.098	120.8	120.1	120.0
C4a–C9a–C9	124.5 (2)	123.733	125.3	125.0	124.8
C4a–C9a–C1	118.7 (2)	119.031	118.5	118.9	119.4
C9–C9a–C1	116.7 (2)	119.274	116.2	116.1	115.8
S1–C4a–C9a	122.9 (2)	121.988	122.1	122.6	122.4
S1–C4a–C4	116.1 (2)	119.708	116.4	116.6	116.9
C9a–C4a–C4	121.0 (2)	119.042	121.5	120.9	120.7
O9–C9–C8a	119.4 (2)	120.777	119.2	119.9	119.9
O9–C9–C9a	120.9 (2)	120.777	119.3	120.1	120.0
C8–C9–C9a	119.6 (2)	117.662	121.5	119.9	120.2
C10a–C5–C6	120.3 (2)	119.864	120.0	120.2	120.1
C8–C7–C6	119.2 (2)	120.156	119.6	119.6	119.4
C8a–C8–C7	121.7 (2)	119.802	121.3	121.4	121.1
C4a–C4–C3	117.7 (2)	118.384	117.6	117.8	117.7
C4a–C4–C41	120.9 (2)	122.224	121.8	122.0	122.2
C3–C4–C41	121.4 (2)	119.948	120.5	120.3	120.0
C4–C3–C2	122.0 (2)	120.836	121.8	122.0	122.2
C9a–C1–C2	120.8 (2)	119.802	120.8	120.9	120.6
C42–C41–C43	109.6 (2)	110.553	110.5	111.0	111.1
C42–C41–C4	110.5 (2)	111.849	110.7	110.7	110.8
C43–C41–C4	113.5 (2)	111.849	113.5	113.4	113.2
C3–C2–C1	119.8 (2)	120.280	119.7	119.6	119.4
C5–C6–C7	120.4 (2)	120.156	120.1	120.3	120.4
RMSD			0.7	0.5	0.6

feld surface shows the relative contribution of the intermolecular contacts present in each compound (Fig. 3S, in Supplementary material) [23]. In the crystal structure, the higher contribution occurs to H···H contacts (57.6%). The C···H contacts account for 14.5% of the Hirshfeld surface, a slightly larger value compared with that of C···C (12.3%). These three kinds of contacts emphasize the significant occurrence of van der Waals and π–π interactions [28]. Accordingly, the hydrophilic O···H contact contributions to the crystal structure is 9%. In addition, the smallest 2D-fingerprint contributions occur for S···H (4.9%), C···O (0.8%), C···S (0.7%) and S···O (0.4%) contacts. Finally, the examination of the Hirshfeld surface demonstrates that there are no contributions for S···S and O···O halogen contacts. In the crystal packing of 4-ITX, the molecules are assembled to form layers parallel the $(40\overline{2})$ plane (Fig. S4, in Supplementary material).

3.2. Molecular electrostatic potential map

The molecular electrostatic potential (MEP) was obtained after the Gaussian calculations using the DFT available in the Gaussian 03 W [10], investigated under B3LYP/6-311G(d,p) optimized geometry, and visualized with the Molekel program [31]. The existence of the mentioned intermolecular interactions of 4-ITX can be supported by the calculated MEP map (Fig. 4), a useful tool to visualize charge distribution in molecules, indicating regions suitable to participate in intermolecular interactions as a donor and acceptor of hydrogen bonds. The positive regions (blue) of 4-ITX are basically localized on Cg3, followed by less positive regions located on the aromatic hydrogen atoms (except H1 and H8 atoms) and two CH_3 of isopropyl group with electrophilic reactivity. The negative (red and yellow) regions are observed mainly around the O9

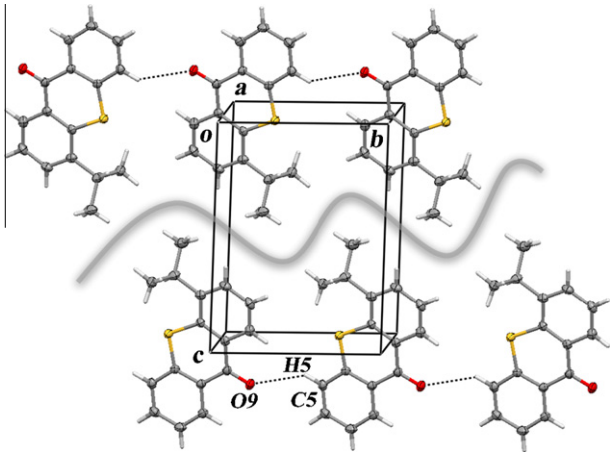

Fig. 2. Illustration of 1-D chains occurring along the *b* axis linked by weak intermolecular interactions. The hydrophobic regions are also emphasized.

Table 3
Hydrogen-bonding lengths (Å) and angles (°) for 4-ITX. *'D' and 'A' mean* hydrogen bond donor–acceptor, respectively.

D–H···A	D–H	H···A	D···A	D–H···A
C5–H5···O9[a]	0.93	2.60	3.364(3)	140
C42–H42···O9[b]	0.96	2.52	3.387(3)	150

Symmetry codes:
[a] *x*, 1 + *y*, *z*.
[b] 1 − *x*, −*y*, −*z*.

atom of the carbonyl group with nucleophilic reactivity. Hence, the MEP map clearly shows the possibility of occurrence of intermolecular interactions in 4-ITX. The negative regions around the O9 atom highlight its participation as a proton acceptor in two intermolecular hydrogen bonds in the crystal structure (Table 3). Therefore, it can be inferred from Fig. 4 that hydrogen bonds (C–H···O bonds) can be formed between the stronger electron donors (O9 atom) and the regions of positive potential on the aromatic and isopropylic hydrogen atoms from the adjacent molecules, which act as a moderate proton donor. The positive regions of MEP map, which are centered mainly on Cg3 compared with Cg1 and Cg2, can be an explanation for the π–π stacking geometry observed in Fig 3b. As a result, in the 4-ITX structure, it is most favorable π–π interactions linking the centroid Cg3 to Cg1 or Cg2 (with less positive potential) than Cg3 accepting π-electrons of another Cg3 adjacent (with most positive potential).

3.3. Thermodynamic properties

The thermodynamic properties obtained from theoretical studies of 4-ITX are shown in Table S4, in Supplementary material. The total energy of the system is higher for the HF method when compared to the DFT method, whereas the zero point energy has a greater value when using the 6-31++G basis for the level of DFT. The rotational constants calculated were the same for both methods used in this study. The value of entropy is higher for B3LYP/6-311G(d,p) when compared with the other basis sets and the HF method. For the dipole moment, the DFT method results are similar, whereas for the HF method the value is smaller. These thermodynamic parameters clearly play an important role in describing the vibrational motion and the behavior of the compound.

3.4. Infrared spectroscopy

The structural features of 4-ITX were also analyzed by experimental FT-IR spectroscopy and the theoretical IR data providing important insights to understand the structural properties of 4-ITX in the solid state. This molecule has 32 atoms and 90 normal modes of fundamental vibration and the description of vibrational modes can be given by means of normal coordinate analysis. The detailed vibrational assignments are achieved by comparing the band positions and intensities observed in FT-IR spectra with wavenumbers and intensities reported in the literature, and from molecular modeling calculations at B3LYP/6-311G(d,p) and B3LYP/6-31++G level [32]. The best match between theoretical and experimental data was obtained using B3LYP/6-311G(d,p). Accordingly, this method was used to further comparisons. The calculated vibrational wavenumbers were scaled with the scale factor obtained from the correlation between the key experimental and computed wavenumbers for 4-ITX (Fig. S5, in Supplementary material). The experimental and scaled theoretical infrared spectra of 4-ITX are shown in Fig. 5.

The carbonyl stretching receives special attention because of their characteristic band in thioxanthone [33,34] and xanthone derivatives [35], a class of chemical compounds that differ from thioxanthones exchanging the oxygen heteroatom for a sulfur atom. In the present study, for the 4-ITX, was found the experimental *ν*C=O axial stretching at 1630 cm^{-1}, which is closer than the calculated frequencies obtained for B3LYP/6-311G(d,p) method, presenting the value of 1629 cm^{-1}. With regard to the endocyclic sulfur, it can be seen that the experimental C–S stretching vibration was attributed to a very weak band at 777 cm^{-1}, while the theoretical calculations predicted this mode at 786 cm^{-1} for the B3LYP/6-311G(d,p) method.

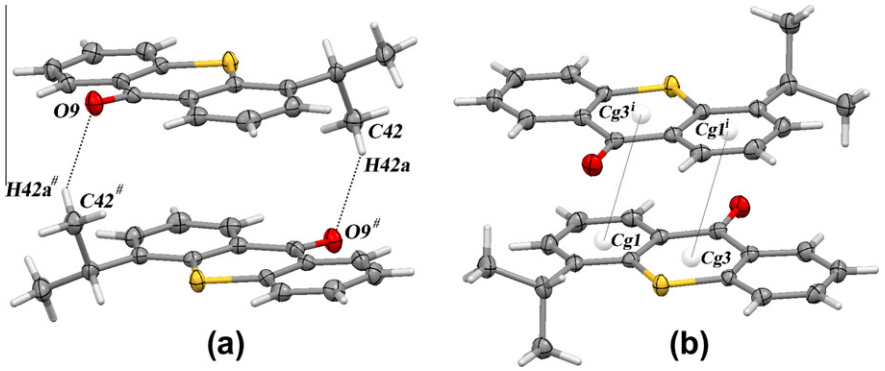

Fig. 3. Representation of weak intermolecular interactions occurring in 4-ITX. (a) Non-classical H-bond (symmetry code: #1 − *x*, *y*, *z*) and (b) face-to-face π–π interaction (symmetry code: *i* = −*x*, −*y*, −*z*).

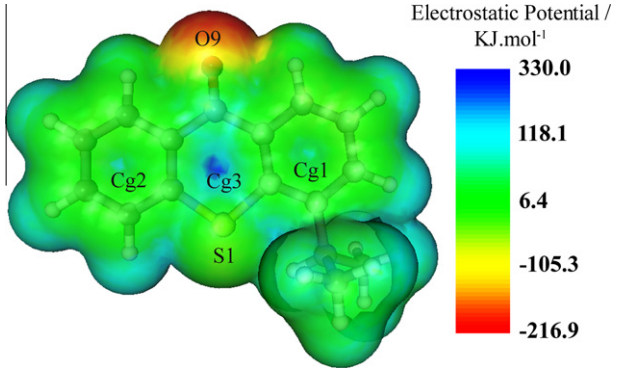

Fig. 4. Molecular electrostatic potential map calculated at B3LYP/6-311G(d,p). Red indicates a value greater than or equal to the maximum in negative potential and blue indicates a value greater than or equal to the maximum in positive potential. (For interpretation of the references to colour in this figure legend, the reader is referred to the web version of this article.)

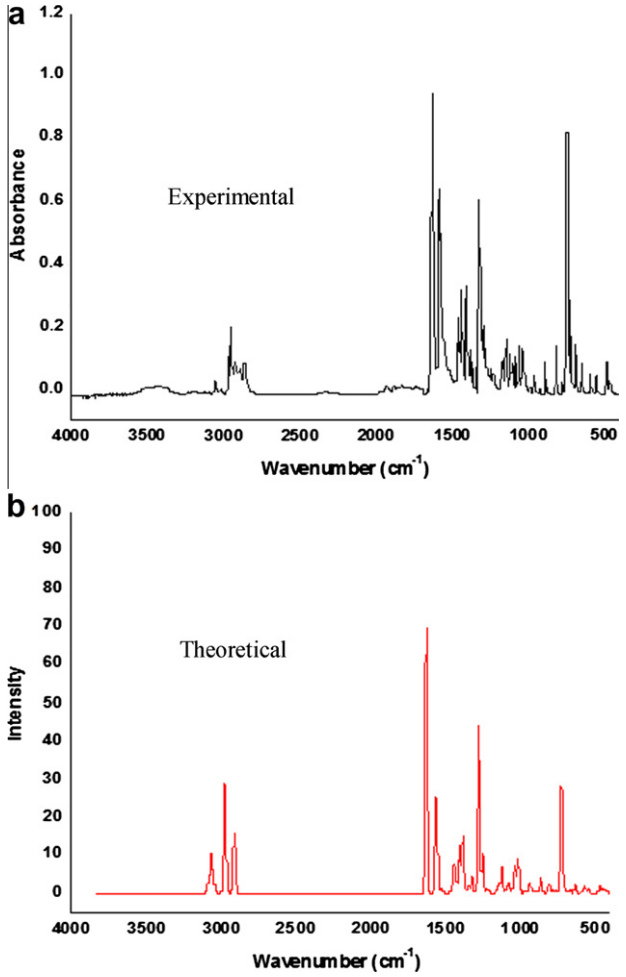

Fig. 5. Infrared spectra of 4-ITX. (a) Experimental FT-IR in KBr and (b) scaled theoretical data using B3LYP/6-311G(d,p).

In the 4-ITX, the experimental C–H aromatic stretching vibrations are assigned to a weak band in the region of 3065 cm^{-1}, which is similar considering the computed frequencies in the B3LYP/6-311G(d,p) method occurring around 3066 cm^{-1}. Also, a weak combination and overtone bands in the experimental spectrum appear between 1977 and 1966 cm^{-1}. In plane deformations, the experimental and the computed data are 1325 and 1280 cm^{-1}, respectively. The bands occurring at low-frequencies (ranging 894–688 cm^{-1}) are related to out-of-plane deformations of the C–H aromatic groups, while these bands are predicted to be in between 868 and 672 cm^{-1} by theoretical calculation.

The C–H stretching vibration tertiary is very weak. Experimentally, it was attributed to a band at 2897 cm^{-1}, and the CH_3 asymmetric stretching vibrations were associated to the band at 2956 cm^{-1}, whereas the band at 2869 cm^{-1} was assigned to the CH_3 symmetric stretching vibrations of the two methyl substituents of isopropyl. According to a theoretical analysis, these bands are displaced around 2975 cm^{-1}, a region with overlaps among them. The bands at 1463 and 1436 cm^{-1} are assigned to the asymmetric deformations vibrations of the methyl group because the calculations predicted those modes at 1449 and 1439 cm^{-1}. In addition, as predicted by theoretical calculations, the CH_3 symmetric deformation vibrations is assigned to the band at 1380 cm^{-1} in the experimental data.

3.5. ^{1}H and $^{13}C\{^{1}H\}$ NMR analysis

In the ^{1}H NMR experiment, the chemical shifts of the most acid aromatic protons (H1 and H8) are found in the 8.61 and 8.53 ppm regions, respectively. The other aromatic protons (H2, H3, H5, H6 and H7) are magnetically similar, giving rise to a complex set of multiplet signals ranging 7.64–7.47 ppm [34]. Analyzing the isopropyl group, the hydrogen linking to C41 atom exhibits a septet signal in 3.49 ppm (J = 6.76 Hz). In addition, the signals related to the six hydrogen atoms of the methyl groups (C42 and C43) appear as doublet in 1.40 ppm (J = 6.76 Hz). Probably, this is an evidence of the non-equivalence among the protons of each methyl group, as observed above according to the crystal structure and theoretical optimization. Moreover, in the $^{13}C\{^{1}H\}$ NMR experiment, the chemical shift of the carbonyl group appear at 180.8 ppm, which is slightly different from that of the thioxanthone molecule (180.1 ppm) [36]. Other five signals of low intensity are observed, and they can be attributed to those carbon atoms non-hydrogenated named as C4, C4a, C10a, C9a, and C8a, which present the values of 144.62, 136.96, 135.41, 129.80, and 128.62 ppm, respectively. The remaining aromatic hydrogenated carbon atoms were also identified in the range of 132.3–126.0 ppm. Finally, the other more shielded atoms, including the methylene (30.0 ppm) and the two methyl groups (23.0 ppm), present characteristic chemical shifts [36]. In such case, it was not possible to distinguish the two methyl groups given that a broad signal is observed.

3.6. UV spectroscopy

The UV–Vis absorption spectra of 4-ITX were measured in a solution of dichloromethane, tetrahydrofuran and methanol (1.0×10^{-4} M). The computed UV–Vis was processed using the TD-DFT method at the B3LYP and 6-311G(d,p) basis set in Gaussian 03 W software package [10]. The main results of experimental and TD-DFT calculated absorptions are summarized in Table 4. In each solvent, the experimental spectrum presents two maximum absorption bands between 305 and 385 nm, whereas the TD-DFT results predict these bands around 286 and 360 nm (Table 4). Experimentally, the long-wavelength maximum shifts towards high energy when the solvent polarity is increased, in agreement with previous reports [37,38]. Probably, the different interactions between chromosphere regions of 4-ITX and the solvent are responsible for this slight shift observed. However, this tendency is not observed in the TD-DFT data. Comparing the experimental and the TD-DFT results shown in Table 4, it is observed a reasonable concordance between the wavelengths. The band found in

Table 4
Experimental and theoretical electronic absorption values for 4-ITX in different solvents.

Solvent	Experimental	B3LYP/6-311G(d,p)			
	λ (nm)	λ (nm)	Transition energy (eV)	Oscillator strength	Transition character
Dichloromethane	388	360.5	3.4397	0.0976	HOMO – LUMO
	306	286.2	3.7042	0.0169	HOMO – LUMO + 1
Tetrahydrofuran	384	360.0	3.4440	0.0964	HOMO – LUMO
	306	286.1	4.3331	0.0176	HOMO – LUMO + 1
Methanol	384	361.2	3.4326	0.0918	HOMO – LUMO
	302	286.6	4.3261	0.0112	HOMO – LUMO + 1

the region of 361.2–360.0 nm varying the solvent can be assigned to the $\pi \rightarrow \pi^*$ transition from HOMO to LUMO, in which the carbonyl and endocyclic sulfur are involved in the electronic transition (Fig. S8, in Supplementary material). In addition, the UV absorption band at 286 nm of 4-ITX results from an electronic transition from HOMO to LUMO + 1, with the LUMO + 1 localized mainly on the aromatic rings A and B. This supports the interpretation that the characteristic UV absorption at 286 nm is contributed by the $\pi \rightarrow \pi^*$ transition of the two aromatic systems. The transition from HOMO to LUMO + 1 does not involve the carbonyl group or the sulfur atom, as can be seen in the Fig. S8.

4. Conclusion

In summary, a detailed analysis of 4-ITX was performed according to its crystal structure, theoretical and experimental infrared, ^{1}H and ^{13}C{^{1}H} NMR, and UV–Vis absorption. The geometric parameters of 4-ITX obtained using the B3LYP/6-311G(d,p) method match well with the X-ray diffraction data. In both theoretical and experimental studies, the three fused rings adopt a planar conformation and the isopropyl group in a most stable orientation. In addition, the crystallographic analysis reveals the influence of C–H···O intermolecular hydrogen bonds and resonance on the increase in the carbonyl bond length. The hydrogen bonds in the 4-ITX compound were supported by calculation of the molecular electrostatic potential (MEP), where the negative potential located on O9 atom highlights its behavior as a strong proton acceptor region. The crystal self-assembly of 4-ITX is also kept together by van der Waals and π–π interactions. In the UV–Vis study, the red shift that increases the solvent polarity is attributed to $\pi \rightarrow \pi^*$ transition. The knowledge obtained from the present study will be useful in further analysis of other thioxanthone and similar derivatives, and it will certainly aid future investigation of structure–activity relationships and electronic properties.

Acknowledgment

The authors gratefully acknowledge the financial support provided by FAPESP, CNPq and CAPES/PROEX. R.S. Corrêa acknowledges the FAPESP Ph.D. fellowship 2009/08131-1.

Appendix A. Supplementary material

Figs. S1–S8 and Tables S1–S4. The crystallographic data for the structural analysis reported in this article have been deposited at the Cambridge Crystallographic Data Center, CCDC 810206. Copies of this information may be obtained free of charge from the Director, CCDC, 12 Union Road, Cambridge CB2 1EZ, UK. Fax: +44 01223 336 033, e-mail: deposit@ccdc.cam.ac.uk or http://www.ccdc.com.ac.uk/deposit. Supplementary data associated with this article can be found, in the online version, at doi:10.1016/j.molstruc.2011.06.016.

References

[1] F. Catalina, C. Peinado, R. Sastre, J.L. Mateo, J. Photochem. Photobiol. A 47 (1989) 365.
[2] F. Catalina, C. Peinado, N.S. Allen, J. Photochem. Photobiol. A 67 (1992) 255.
[3] D. Sevinc, F. Karasu, N. Arsu, J. Photochem. Photobiol. A 203 (2009) 81.
[4] N. Arsu, M. Aydin, Y. Yagci, S. Jockusch, N.J. Turro, in: J.P. Fouassier (Ed.), Photochemistry and UV Curing: New Trends, Research Signpost, Trivandrum, 2006.
[5] C. Roffey, Photogeneration of reactive species for UV-curing, Wiley, Sussex, UK, 1997.
[6] A. Gil-Vergara, C. Blasco, Y. Picó, Anal. Bioanal. Chem. 389 (2007) 605.
[7] H. Gallart-Ayala, E. Moyano, M.T. Galceran, J. Chromatogr. A 1208 (2008) 182.
[8] M.P. Wentland, R.B. Pemi, J.I. Huang, R.G. Powles, S.C. Aldous, K.M. Klingbeil, A.D. Peverly, R.G. Robinson, T.H. Corbett, J.L. Jones, J.B. Rake, S.A. Coughlin, Bioorg. Med. Chem. Lett. 6 (1996) 1345.
[9] P.H. Goncalves, F. High, P. Juniewicz, G. Shackleton, J. Li, S. Boerner, P.M. LoRusso, Invest. New Drugs 26 (2008) 347.
[10] GAUSSIAN03W, Revision C.02, M.J. Frisch, G.W. Trucks, H.B. Schlegel, G.E. Scuseria, M.A. Robb, J.R. Cheeseman, V.G. Zakrzewski, J.A. Montgomery, R.E. Stratmann, J.C. Burant, S. Dapprich, J.M. Millam, A.D. Daniels, K.N. Kudin, M.C. Strain, O. Farkas, J. Tomasi, V. Barone, M. Cossi, R. Cammi, B. Mennucci, C. Pomelli, C. Adamo, S. Cliord, J. Ochterski, G.A. Petersson, P.Y. Ayala, Q. Cui, K. Morokuma, D.K. Malick, A.D. Rabuck, K. Raghavachari, J.B. Foresman, J. Cioslowski, J.V. Ortiz, B.B. Stefanov, G. Liu, A. Liashenko, P. Piskorz, I. Komaromi, R. Gomperts, R.L. Martin, D.J. Fox, T. Keith, M.A. Al-Laham, C.Y. Peng, A. Nanayakkara, C. Gonzalez, M. Challacombe, P.M.W. Gill, B. Johnson, W. Chen, M.W. Wong, J.L. Andres, M. Head-Gordon, E.S. Replogle, J.A. Pople, GAUSSIAN03 program, Gaussian Inc., Pittsburgh, PA, 2003.
[11] C. Moller, M.S. Plesset, Phys. Rev. 46 (1934) 618.
[12] P. Hohenberg, W. Khon, Phys. Rev. B 136 (1964) 864.
[13] A.D. Becke, J. Chem. Phys. 98 (1993) 5648.
[14] C. Lee, W. Yang, R.G. Parr, Phys. Rev. B 37 (1998) 785.
[15] Enraf-Nonius COLLECT. Nonius BV, Delft, The Netherlands, 1997–2000.
[16] Z. Otwinowski, W. Minor, in: C.W. Carter Jr., R.M. Sweet (Eds.), Methods in Enzymology, vol. 276, Academic Press, New York, 1997, p. 307.
[17] G.M. Sheldrick, Acta Crystallogr. A 64 (2008) 112.
[18] L.J. Farrugia, J. Appl. Crystallogr. 32 (1999) 837.
[19] L.J. Farrugia, J. Appl. Crystallogr. 30 (1997) 565.
[20] I.J. Bruno, J.C. Cole, P.R. Edgington, M.K. Kessler, C.F. Macrae, P. McCabe, J. Pearson, R. Taylor, Acta Crystallogr. B 58 (2002) 389.
[21] I.J. Bruno, J.C. Cole, M. Kessler, J. Luo, W.D.S. Motherwell, L.H. Purkis, B.R. Smith, R. Taylor, R.I. Cooper, S.E. Harris, A.G. Orpen, J. Chem. Inf. Comput. Sci. 44 (2004) 2133.
[22] F.H. Allen, Acta Crystallogr. B 58 (2002) 380.
[23] S.K. Wolff, D.J. Grimwood, J.J. McKinnon, D. Jayatilaka, M.A. Spackman, CrystalExplorer 2.1, University of Western Australia, Perth, 2007.
[24] M.F. Richardson, R.S. Guzowski, J. Cryst. Spectrosc. 23 (8) (1993) 633.
[25] J.W. Brock, S.G. Bott, J. Chem. Crystallogr. 25 (6) (1995) 321.
[26] S.S.C. Chu, V. Napoleone, Cryst. Struct. Commun. 11 (1982) 291.
[27] S.S.C. Chu, Acta Crystallogr. B 32 (1976) 1583.
[28] R.S. Corrêa, M.H. dos Santos, T.J. Nagem, J. Ellena, Struct. Chem. 21 (2010) 555.
[29] R.S. Corrêa, C.P. Coelho, M.H. dos Santos, J. Ellena, A.C. Doriguetto, Acta Crystallogr. C 65 (2009) 97.
[30] A.A. Pimenta, S. Silva, G.D. Silva, L. Barbosa, J. Ellena, A.C. Doriguetto, Struct. Chem. 17 (2006) 149.
[31] MOLEKEL 4.0, P. Flúkiger, H.P. Lúthi, S. Portmann, J. Weber, Swiss Center for Scientific Computing, Manno Switzerland, 2000.
[32] N. Sundaraganesan, G. Elango, C. Meganathan, B. Karthikeyan, M. Kurt, Mol. Simulat. 35 (9) (2009) 705.
[33] R.E. Connors, C.M. Fratini, J. Mol. Struct. 553 (2000) 235.
[34] R.H. Martin, N. Defay, F. Geerts-Evrard, P.H. Given, J.R. Jones, R.W. Wedel, Tetrahedron 21 (1965) 1833.
[35] N.S. Gonçalves, R. Cristiano, M.G. Pizzolatti, F.S. Miranda, J. Mol. Struct. 733 (2005) 53.
[36] I.W.J. Still, N. Plavac, D.M. Mckinnon, M.S. Chauhan, Can. J. Chem. 54 (1976) 280.
[37] G.C. Ferreira, C.C. Schmitt, M.G. Neumann, J. Brazil. Chem. Soc. 17 (2006) 905.
[38] C. Peinado, F. Catalina, T. Corrales, R. Sastre, F. Amat-Guerri, N.S. Allen, Eur. Polym. J. 28 (10) (1992) 1315.